

A Novel Framework Using Variational Inference with Normalizing Flows to Train Transport Reversible Jump Proposals

Pingping Yin¹ Xiyun Jiao¹

Abstract

We propose a unified framework that employs variational inference (VI) with (conditional) normalizing flows (NFs) to train both between-model and within-model proposals for reversible jump Markov chain Monte Carlo, enabling efficient trans-dimensional Bayesian inference. In contrast to the transport reversible jump (TRJ) of Davies et al. (2023), which optimizes forward KL divergence using pilot samples from the complex target distribution, our approach minimizes the reverse KL divergence, requiring only samples from a simple base distribution and largely reducing computational cost. Especially, we develop a novel trans-dimensional VI method with conditional NFs to fit the conditional transport proposal of Davies et al. (2023). We use RealNVP flows to learn the model-specific transport maps used for constructing proposals so that the calculation is parallelizable. Our framework also provides accurate estimates of marginal likelihoods, which may facilitate efficient model comparison and help design rejection-free proposals. Extensive numerical studies demonstrate that the TRJ method trained under our framework achieves faster mixing compared to existing baselines.

1. Introduction

Many inference problems have a trans-model nature, such as variable selection (Fan et al., 2026), phylogenetic tree search (Jiao et al., 2021), geoscientific inversion (Sambridge et al., 2013), etc. Denote the data by \mathbf{y} and suppose there are K (≥ 2) candidate models for \mathbf{y} . Each model k has a vector of d_k parameters $\boldsymbol{\theta}_k \in \Theta_k \subset \mathbb{R}^{d_k}$, where d_k may vary with k . Then the unknown parameter of the trans-model inference problem is $(k, \boldsymbol{\theta}_k)$, with the state space $\Omega = \bigcup_{k=1}^K (\{k\} \times \Theta_k)$, i.e., the union of the subspaces for

¹Department of Statistics and Data Science, Southern University of Science and Technology, Shenzhen, Guangdong, China. Correspondence to: Xiyun Jiao <jiaox@ustech.edu.cn>.

Preprint. February 5, 2026.

the K models. The joint posterior distribution of $(k, \boldsymbol{\theta}_k)$ is

$$\pi(k, \boldsymbol{\theta}_k \mid \mathbf{y}) \propto \pi(k) \pi(\boldsymbol{\theta}_k \mid k) \pi(\mathbf{y} \mid \boldsymbol{\theta}_k, k), \quad (1)$$

where $\pi(k)$ is the prior of model index k , $\pi(\boldsymbol{\theta}_k \mid k)$ and $\pi(\mathbf{y} \mid \boldsymbol{\theta}_k, k)$ are the prior and likelihood under model k .

Reversible jump Markov Chain Monte Carlo (RJMCMC, GREEN, 1995), a generalization of Metropolis-Hastings, is designed to sample from trans-model posteriors as eq. (1). It is notoriously difficult for RJMCMC to achieve reasonable acceptance rate and mixing efficiency when moving between models. Strategies to design efficient trans-model proposals include constructing multivariate Gaussian proposals analogous to random walks with informative mean and variances (Green, 2003), estimating conditional marginal densities (Fan et al., 2009), using KD-tree approximation of the target densities for auxiliary-variable draws (Farr et al., 2015), locally-informed proposals for model index (Gagnon, 2021), etc. Other approaches to encouraging trans-model jumps involve multi-step proposals (Green & Mira, 2001; Al-Awadhi et al., 2004) and saturated-space methods (Brooks et al., 2003). However, none of these methods are general enough to be widely applied in practice.

Davies et al. (2023) extended the idea of using measure transports to accelerate MCMC in recent work (Parno & Marzouk, 2018; Hoffman et al., 2019; Gabrié et al., 2021) into trans-model scenarios, and successfully developed a general method for constructing efficient trans-dimensional proposals, named by *transport reversible jump* (TRJ). To propose from model k to k' , TRJ first (approximately) transports $\boldsymbol{\theta}_k$ from the conditional posterior $\pi_k = \pi(\cdot \mid k, \mathbf{y})$ to an auxiliary variable \mathbf{z}_k from some easy-to-sample *reference* distribution, proposes in the reference space to get a new candidate $\mathbf{z}_{k'}$ with dimension $d_{k'}$, and then transports $\mathbf{z}_{k'}$ to $\boldsymbol{\theta}_{k'}$, which is approximately $\pi_{k'}$ -distributed. Davies et al. (2023) proved that if the transports are exact, the resulting algorithm has the same acceptance probability as performing marginal MCMC on the space of model index.

Davies et al. (2023) fitted the approximate TMs by minimizing the forward KL divergence so that pilot samples from the target posteriors are required. Thus the accuracy for approximating the TMs and the efficiency of the corresponding algorithms highly depend on the quality of the

pilot samples. Moreover, Davies et al. (2023) approximated transport maps (TMs) using the *autoregressive flow* (AF) model. The sequential nature of AFs makes the inverse sampling procedure non-parallelizable, which largely limits the computational efficiency.

In this work, inspired by Hoffman et al. (2019), which uses variational inference (VI) to fit TMs, we utilize VI with NFs (Rezende & Mohamed, 2015) to train TRJ proposals and further improve the efficiency of RJMCMC.

Our main contributions are

- We propose a unified framework (Algorithm 3 in Appendix A) using VI to train TM-based between-model and within-model proposals with TMs specified by NFs, so that pilot samples from the complex target posteriors are not required. We construct the approximate TMs using the real-valued non-volume preserving (RealNVP, Dinh et al., 2017) transformation, which is more efficient than AFs in computation. Accurate marginal likelihood estimates, which may facilitate model comparison and rejection-free proposal design, are by-products of our framework.
- We develop a novel trans-dimensional VI method with conditional NFs to fit the conditional transport proposal of Davies et al. (2023), which learns the approximate TMs for all the models by training just once.
- We use extensive numerical studies including those in Davies et al. (2023) to demonstrate that our methods lead to better mixing and faster convergence compared to existing baseline algorithms.

Code for numerical experiments is available at <https://github.com/Palantir-zoe/vinftrjp>.

The remainder of the paper is organized as follows. In Section 2, we review RJMCMC, TRJ proposals, VI with NFs, and RealNVP versus AFs. In Section 3, we introduce our framework using VI with NFs to train both between-model and within-model proposals of RJMCMC. In Section 4, we use numerical examples to show the efficacy of our new methods. We conclude in Section 5.

2. Background

2.1. Reversible Jump Markov Chain Monte Carlo

To propose a move from $\omega = (k, \theta_k)$ to $\omega' = (k', \theta_{k'})$, where the dimensions of θ_k and $\theta_{k'}$ are d_k and $d_{k'}$, RJMCMC first proposes a new model k' with probability $q(k'|k)$. To solve the problem that d_k and $d_{k'}$ may be different, RJMCMC utilizes *dimension matching*, that is, introducing auxiliary variables $\mathbf{u}_k \sim \varphi_k$ and $\mathbf{u}_{k'} \sim \varphi_{k'}$ of dimensions m_k

and $m_{k'}$, such that $d_k + m_k = d_{k'} + m_{k'}$. Then a proposal of $\theta_{k'}$ is generated by using \mathbf{u}_k , $\mathbf{u}_{k'}$ and a diffeomorphism $g_{k,k'}$ so that $(\theta_{k'}, \mathbf{u}_{k'}) = g_{k,k'}(\theta_k, \mathbf{u}_k)$. The new proposal $(k', \theta_{k'})$ is accepted with probability

$$\alpha(\omega, \omega') = \min \left\{ 1, \frac{\pi(\omega'|\mathbf{y})\varphi_{k'}(\mathbf{u}_{k'})q(k|k')}{\pi(\omega|\mathbf{y})\varphi_k(\mathbf{u}_k)q(k'|k)} |J_{k,k'}| \right\}, \quad (2)$$

where $J_{k,k'} = \frac{\partial g_{k,k'}(\theta_k, \mathbf{u}_k)}{\partial(\theta_{k'}, \mathbf{u}_{k'})}$ is the Jacobian matrix and $|\cdot|$ the absolute value of determinant. The choices of φ_k , $\varphi_{k'}$ and $g_{k,k'}$ have large impact on the efficiency of RJMCMC.

2.2. Transport Reversible Jump Proposals

For model k , if $T_k : \mathbb{R}^{d_k} \rightarrow \mathcal{Z}^{d_k}$ is a TM from π_k to $\otimes_{d_k} \nu$, i.e., a reference distribution defined on \mathcal{Z}^{d_k} , then $T_k \# \pi_k = \otimes_{d_k} \nu$. Note that $\otimes_{d_k} \nu$ is the joint density of d_k independent ν -distributed variables, with ν to be some univariate distribution defined on $\mathcal{Z} \subset \mathbb{R}$.

TRJ utilizes the TMs $\{T_k\}$ to make trans-model proposals. Given (approximated) TMs for all the models, TRJ proposes a move from k to k' by first transporting the current parameters θ_k in model k to the reference space, i.e.,

$$\mathbf{z}_k = T_k(\theta_k). \quad (3)$$

If $d_{k'} \geq d_k$, an auxiliary variable \mathbf{u}_k of dimension $d_{k'} - d_k$ is drawn from $\otimes_{d_{k'} - d_k} \nu$, and a diffeomorphism $\bar{h}_{k,k'}$ is applied on the concatenated vector of \mathbf{z}_k and \mathbf{u}_k to obtain a reference variable $\mathbf{z}_{k'}$ corresponding to model k' , that is,

$$\mathbf{z}_{k'} = \bar{h}_{k,k'}(\mathbf{z}_k, \mathbf{u}_k). \quad (4)$$

If $d_{k'} < d_k$, $\mathbf{u}_{k'}$ of dimension $d_k - d_{k'}$ is discarded from \mathbf{z}_k before applying $\bar{h}_{k,k'}$. Note that $\bar{h}_{k,k'}$ should satisfy the pushforward-invariance and volume-preserving conditions and a default choice is the identity map (Davies et al., 2023). Finally, a parameter value in model k' is proposed by

$$\theta_{k'} = T_{k'}^{-1}(\mathbf{z}_{k'}). \quad (5)$$

Davies et al. (2023) proved that if all the TMs are exact, then the TRJ proposals are in some sense optimal, with the acceptance probability in eq. (2) reduced to:

$$\alpha(\omega, \omega') = \min \left\{ 1, \frac{\pi(k'|y)q(k|k')}{\pi(k|y)q(k'|k)} \right\}, \quad (6)$$

which depends on model index alone.

Davies et al. (2023) used several chained AF models (details in Section 2.4) to approximate TMs, and trained them by minimizing the forward Kullback-Leibler (KL) divergence between the AF model and an empirical distribution estimated using the pilot samples from the target. The approximate TMs can be fitted for each model individually, but

the computational cost is high if the number of models K is large. To solve this problem, Davies et al. (2023) introduced the *conditional transport proposal* (CTP), which can obtain all the approximate TMs by training just once. Specifically, CTP considers the *saturated-space* approach (Brooks et al., 2003) and augments the state space of each model to the maximum dimension $d_{max} = \max_{k \in \{1, 2, \dots, K\}} \{d_k\}$. The augmented target distribution is

$$\tilde{\pi}(\tilde{\omega}) = \pi(\omega | \mathbf{y}) (\otimes_{d_{max} - d_k} \nu)(\mathbf{u}_{\sim k}), \quad (7)$$

where $\omega = (k, \theta_k)$, $\tilde{\omega} = (k, \theta_k, \mathbf{u}_{\sim k})$ and the auxiliary variable $\mathbf{u}_{\sim k}$ of dimension $d_{max} - d_k$ is drawn from a reference distribution $\otimes_{d_{max} - d_k} \nu$. In this setting, all the approximate TMs $\{\tilde{T}(\cdot | k)\}$ can be learned by training one single *conditional* NF given the model index k as an input (context). The proposal from model k to k' is constructed by first drawing k' from $q(\cdot | k)$ and then letting $(\theta_{k'}, \mathbf{u}_{\sim k'}) = c_{k'}^{-1} \circ \tilde{T}^{-1}(\cdot | k') \circ \tilde{T}(\cdot | k) \circ c_k(\theta_k, \mathbf{u}_{\sim k})$, where “ \circ ” represents composition, and c_k is concatenation.

2.3. Variational Inference with Normalizing Flows

Variational inference is an optimization approach to approximating posterior distributions (Blei et al., 2017). Given a distribution family \mathcal{Q} , VI searches for the member $q^*(\cdot) \in \mathcal{Q}$ minimizing the KL divergence to the target $\pi(\cdot | \mathbf{y})$, that is,

$$q^*(\theta) = \arg \min_{q(\theta) \in \mathcal{Q}} \text{KL}[q(\theta) \| \pi(\theta | \mathbf{y})]. \quad (8)$$

As the KL divergence in eq. (8) depends on the logarithm of the marginal likelihood (evidence), i.e., $\log \pi(\mathbf{y})$, which is however difficult to compute, VI instead optimizes the *evidence lower bound* (ELBO), that is

$$\text{ELBO}(q) = \mathbb{E}_q[\log \pi(\theta, \mathbf{y})] - \mathbb{E}_q[\log q(\theta)]. \quad (9)$$

As $\text{KL}(q \| \pi) = -\text{ELBO}(q) + \log \pi(\mathbf{y})$, minimizing the negative ELBO is equivalent to minimizing the KL divergence.

Simple choices of approximation distributions, such as mean field, may impose severe restriction on the accuracy of VI. Therefore, Rezende & Mohamed (2015) proposed to construct \mathcal{Q} using NFs, which are able to specify flexible and scalable approximate posteriors with arbitrary complexity. While Rezende & Mohamed (2015) explored both finite and infinite flows, we consider only finite flows in this work, and the distribution in \mathcal{Q} is obtained by successively transforming a random variable θ^0 with simple distribution q_0 (e.g., Gaussian) through a chain of L invertible and smooth mappings, that is, $\theta^L = f_L \circ \dots \circ f_2 \circ f_1(\theta^0)$, and the resulting distribution is $\log q_L(\theta^L) = \log q_0(\theta^0) - \sum_{l=1}^L \log |J_{f_l}(\theta^l)|$, where $J_{f_l}(\theta^l) = \frac{\partial f_l(\theta^l)}{\partial \theta^l}$. The complexity of $q_L(\cdot)$ generally increases with L .

2.4. RealNVP versus Autoregressive Flows

Recall that Davies et al. (2023) specified each approximate TM as a chain of AFs. One AF is defined element-wise as

$$T(\mathbf{z})_i = \tau(z_i; \zeta_i(\mathbf{z}_{\sim i}; \psi)), \text{ for } i = 1, 2, \dots, d, \quad (10)$$

where $\tau(\cdot; \xi)$ is a univariate diffeomorphism parametrized by $\xi \in \Xi$ with Ξ being the set of all admissible ξ values, and each of the functions $\{\zeta_i : \mathbb{R}^{i-1} \rightarrow \Xi\}$ is in practice the output of a single neural network that takes $\mathbf{z}_{\sim i}$ as input.

The coupling-based flow model, RealNVP (Dinh et al., 2017), is constructed by stacking a sequence of *affine coupling layers* (ACL). Given an input vector \mathbf{z} of dimension d and $d_0 < d$, the output \mathbf{x} of an ACL has the form of

$$\mathbf{x}_{1:d_0} = \mathbf{z}_{1:d_0}, \quad \mathbf{x}_{d_0+1:d} = \mathbf{z}_{d_0+1:d} \odot \exp(s(\mathbf{z}_{1:d_0})) + t(\mathbf{z}_{1:d_0}), \quad (11)$$

where s and t are scale and translation functions from $\mathbb{R}^{d_0} \rightarrow \mathbb{R}^{d-d_0}$, and \odot is the element-wise product. The Jacobian matrix $\frac{\partial \mathbf{x}}{\partial \mathbf{z}}$ is lower-triangular and the determinant is $\exp \left[\sum_j s(\mathbf{z}_{1:d_0})_j \right]$, which does not involve the Jacobian of either s or t . Therefore s and t can be arbitrarily complex.

3. New Framework Using VI with NFs to Train TM-based RJMCMC Proposals

3.1. TRJ Proposals Trained by VI with Individual NFs

For model k , Davies et al. (2023) specified T_k , the approximate TM from the target π_k to the reference $\otimes_{d_k} \nu$, as AFs and fit it by minimizing the forward KL divergence, i.e.,

$$\text{KL}[\pi(\theta_k | k, \mathbf{y}) \| q(\theta_k)] = \mathbb{E}_{\pi_k} \left[\log \frac{\pi(\theta_k | k, \mathbf{y})}{q(\theta_k)} \right], \quad (12)$$

where $q(\theta_k) = (\otimes_{d_k} \nu)(T_k(\theta_k)) | J_{T_k}(\theta_k)|$. The KL divergence in eq. (12) is an expectation over the conditional target π_k so that samples from π_k are required for training.

We instead learn T_k^{-1} , i.e., TM from the reference to the target, using VI, which minimizes the reverse KL divergence, so that only requiring samples from the reference. We set T_k^{-1} to be RealNVP with parameters η , denoted by f_η , which is a chain of ACLs as in eq. (11). If $\mathbf{z}_k \sim \otimes_{d_k} \nu$, then $\mathbf{z}_\eta = f_\eta(\mathbf{z}_k) \sim q_\eta$, where $q_\eta(\mathbf{z}_\eta) = (\otimes_{d_k} \nu)(\mathbf{z}_k) | J_{f_\eta}(\mathbf{z}_k)|^{-1}$. The VI with NFs minimizes

$$\text{KL}[q_\eta(\mathbf{z}_\eta) \| \pi(\mathbf{z}_\eta | k, \mathbf{y})] = \mathbb{E}_{q_\eta} \left[\log \frac{q_\eta(\mathbf{z}_\eta)}{\pi(\mathbf{z}_\eta | k, \mathbf{y})} \right], \quad (13)$$

which is the reverse KL divergence between q_η and π_k . Recall that VI minimizes eq. (13) by minimizing the negative ELBO, i.e., $\mathbb{E}_{q_\eta} \left[\log \frac{q_\eta(\mathbf{z}_\eta)}{\pi(\mathbf{z}_\eta | k, \mathbf{y})} \right]$, where

$\pi(\mathbf{z}_\eta, \mathbf{y}|k) = \pi(\mathbf{z}_\eta|k)\pi(\mathbf{y}|\mathbf{z}_\eta, k)$ is the un-normalized version of $\pi(\mathbf{z}_\eta|\mathbf{y}, k)$. By applying the reparameterisation trick (Kingma & Welling, 2014), the negative ELBO becomes

$$\ell(\boldsymbol{\eta}) = \mathbb{E}_{\otimes_{d_k} \nu} \left[\log \frac{q_{\boldsymbol{\eta}}(f_{\boldsymbol{\eta}}(\mathbf{z}_k))}{\pi(f_{\boldsymbol{\eta}}(\mathbf{z}_k), \mathbf{y}|k)} \right], \quad (14)$$

which is an expectation over the simple reference distribution $\otimes_{d_k} \nu$. We use stochastic gradient variational inference (SGVI) to optimize eq. (14), see Algorithm 1. The negative ELBO and its gradient required by the algorithm are estimated with samples from $\otimes_{d_k} \nu$. For the numerical studies in this paper, we use ADAM (Kingma & Ba, 2015) as the optimizer \mathcal{P} and set $m = 256$ in Algorithm 1.

Algorithm 1 Stochastic Gradient Variational Inference

```

1: Set the iteration  $t \leftarrow 1$  and negative ELBO  $\ell^{(t)} \leftarrow \infty$ 
2: Initialize  $\boldsymbol{\eta}^{(t)}$ 
3: Initialize optimizer  $\mathcal{P}$  with global learning rate  $\boldsymbol{\xi}^{(0)}$ 
4: repeat
5:   Sample  $\mathbf{z}^i \sim \otimes_{d_k} \nu$ , for  $i = 1, \dots, m$ 
6:    $\mathbf{g}^{(t)} \leftarrow \frac{1}{m} \sum_{i=1}^m \left[ \frac{\partial}{\partial \boldsymbol{\eta}} \log \left( \frac{q_{\boldsymbol{\eta}^{(t)}}(f_{\boldsymbol{\eta}^{(t)}}(\mathbf{z}^i))}{\pi(f_{\boldsymbol{\eta}^{(t)}}(\mathbf{z}^i), \mathbf{y}|k)} \right) \right]$ 
7:   Update the learning rate  $\boldsymbol{\xi}^{(t)}$  and direction  $\Delta \boldsymbol{\eta}^{(t)}$  with  $\mathcal{P}$  using  $\mathbf{g}^{(t)}$ 
8:    $\boldsymbol{\eta}^{(t+1)} \leftarrow \boldsymbol{\eta}^{(t)} - \boldsymbol{\xi}^{(t)} \Delta \boldsymbol{\eta}^{(t)}$ 
9:    $\ell^{(t+1)} \leftarrow \frac{1}{m} \sum_{i=1}^m \left[ \log \left( \frac{q_{\boldsymbol{\eta}^{(t+1)}}(f_{\boldsymbol{\eta}^{(t+1)}}(\mathbf{z}^i))}{\pi(f_{\boldsymbol{\eta}^{(t+1)}}(\mathbf{z}^i), \mathbf{y}|k)} \right) \right]$ 
10:   $t \leftarrow t + 1$ 
11: until  $t > \text{max-iterations}$ 

```

In this paper, we set ν to be standard Gaussian $\mathcal{N}(0, 1)$ so that $\otimes_{d_k} \nu$ is $\mathcal{N}_d(\mathbf{0}, \mathbf{I})$. We also include t distribution (Andrade, 2024) into our code as an option for ν , which may be more suitable than Gaussian if the target is heavy-tailed.

Davies et al. (2023) used the AF model to specify the TM T_k , and set the function $\tau(\cdot; \boldsymbol{\xi})$ in eq. (10) to be masked autoregressive transforms with rational quadratic splines (RQMA, Durkan et al., 2020) so that the model is tractable in both forward and reverse directions. However, the inverse sampling from \mathbf{z}_k to $\boldsymbol{\theta}_k$ using the AF is sequential, with computational cost $\mathcal{O}(d_k)$, and not parallelizable. We instead specify T_k^{-1} with RealNVP, which is tractable in both directions, but much more efficient in computation. For either direction, the evaluation of RealNVP is highly parallelisable and has a cost of $\mathcal{O}(1)$, scaling well with the dimension. Andrade (2024) showed in their numerical studies that evaluating the neural spline flows with 16 layers is more expensive than computing RealNVP with 64 ACLs. RealNVP is also powerful in representation. In theory, RealNVP with $L = 3$ ACLs can be sufficient to produce accurate approximation (Koehler et al., 2021). We specify the functions s and t in ACL to be multi-layer perceptrons (MLP)

and set the depth of each RealNVP to be $L \geq 8$ in numerical examples. Although focusing on RealNVP, we integrate other commonly used flow models into our framework for users to choose, including masked autoregressive flows (Papamakarios et al., 2017), neural spline flows (Durkan et al., 2020), planner flows (Rezende & Mohamed, 2015), etc.

After obtaining T_k^{-1} and T_k for each model k using the VI method described above, our algorithm proceeds identically to TRJ. Given the current state $\boldsymbol{\omega} = (k, \boldsymbol{\theta}_k)$, we sample k' from $q(\cdot|k)$, and generate $\boldsymbol{\theta}_{k'}$ via the steps in eqs. (3)–(5). We set $\bar{h}_{k,k'}$ to be the identity map. The new proposal $\boldsymbol{\omega}' = (k', \boldsymbol{\theta}_{k'})$ is accepted with probability

$$\alpha(\boldsymbol{\omega}, \boldsymbol{\omega}') = \min \left\{ 1, \frac{\pi(\boldsymbol{\omega}' | \mathbf{y}) g_u' q(k|k') |J_{T_k}|}{\pi(\boldsymbol{\omega} | \mathbf{y}) g_u q(k'|k) |J_{T_{k'}}|} \right\}, \quad (15)$$

where $g_u = (\otimes_{d_{k'}-d_k} \nu)(\mathbf{u}_k)$, $g_u' = 1$ if $d_{k'} \geq d_k$, and $g_u = 1, g_u' = (\otimes_{d_k-d_{k'}} \nu)(\mathbf{u}_{k'})$ otherwise.

3.2. New Trans-dimensional VI Method with Conditional NFs for TRJ Proposals

Recall that Davies et al. (2023) introduced CTP to learn the approximate TMs for all the models by training one single conditional AF model. To achieve this by VI, we extend RealNVP to a conditional version and develop a novel trans-dimensional VI method with conditional NFs.

As Davies et al. (2023), we also adopt the saturated-space approach. For each model k , we use an auxiliary variable $\mathbf{u}_{\sim k}$ from the reference distribution $\otimes_{d_{\max}-d_k} \nu$ to augment the state space so that the conditional target becomes

$$\tilde{\pi}(\tilde{\boldsymbol{\theta}}_k | \mathbf{y}, k) \propto \pi(\mathbf{y} | \boldsymbol{\theta}_k, k) \pi(\boldsymbol{\theta}_k | k) (\otimes_{d_{\max}-d_k} \nu)(\mathbf{u}_{\sim k}), \quad (16)$$

where $\tilde{\boldsymbol{\theta}}_k = (\boldsymbol{\theta}_k, \mathbf{u}_{\sim k})$ is of dimension d_{\max} . Then the target distribution of our trans-dimensional VI is

$$\tilde{\pi}(\tilde{\boldsymbol{\theta}}_k, k | \mathbf{y}) = \tilde{\pi}(\tilde{\boldsymbol{\theta}}_k | \mathbf{y}, k) \tilde{\pi}(k | \mathbf{y}), \quad (17)$$

where $\tilde{\pi}(k | \mathbf{y})$ is the marginal distribution of k . If $\tilde{\pi}(k | \mathbf{y}) = \pi(k | \mathbf{y})$, i.e., the posterior model probability, then our target is the same as that in eq. (7), and the marginal distribution of $\tilde{\pi}(\tilde{\boldsymbol{\theta}}_k, k | \mathbf{y})$ with $\mathbf{u}_{\sim k}$ integrated out is the original target $\pi(\boldsymbol{\theta}_k, k | \mathbf{y})$. However, our main goal is to obtain approximation for the conditional $\pi(\boldsymbol{\theta}_k | \mathbf{y}, k)$, so that it is enough to guarantee that the conditional of $\boldsymbol{\theta}_k$ given $\mathbf{u}_{\sim k}$ and k in $\tilde{\pi}$ is $\pi(\boldsymbol{\theta}_k | \mathbf{y}, k)$. Therefore the choice of $\tilde{\pi}(k | \mathbf{y})$ can be arbitrary for our method. In this paper, we set $\tilde{\pi}(k | \mathbf{y})$ to be the uniform distribution on $\{1, 2, \dots, K\}$.

We specify the variational distribution for approximating our target $\tilde{\pi}(\tilde{\boldsymbol{\theta}}_k, k | \mathbf{y})$ to be $\tilde{q}_{\boldsymbol{\eta}}(\tilde{\boldsymbol{\theta}}_k, k) = \tilde{q}_{\boldsymbol{\eta}}(\tilde{\boldsymbol{\theta}}_k | k) \tilde{q}(k)$, and set $\tilde{q}(k) = \tilde{\pi}(k | \mathbf{y})$, so that $\tilde{q}_{\boldsymbol{\eta}}(\tilde{\boldsymbol{\theta}}_k | k)$ is the variational distribution for approximating the conditional $\tilde{\pi}(\tilde{\boldsymbol{\theta}}_k | \mathbf{y}, k)$. To construct $\tilde{q}_{\boldsymbol{\eta}}(\cdot | k)$, we first introduce a conditional RealNVP

model with each ACL to be

$$\begin{aligned} \mathbf{z}_{1:d_0} &= \mathbf{z}_{1:d_0}, \\ \mathbf{x}_{d_0+1:d_{\max}} &= \mathbf{z}_{d_0+1:d_{\max}} \odot \exp(s(\mathbf{z}_{1:d_0}, k)) + t(\mathbf{z}_{1:d_0}, k). \end{aligned} \quad (18)$$

In contrast to the ACL in eq. (11), s and t in eq. (18) are MLPs taking both $\mathbf{z}_{1:d_0}$ and k as inputs. Then we start from a variable $\tilde{\mathbf{z}}_0$ of dimension d_{\max} , which follows a simple base distribution $\tilde{q}_0(\cdot|k)$, and apply the conditional RealNVP $f_{\eta}(\cdot|k)$ with ACLs as in eq. (18) onto $\tilde{\mathbf{z}}_0$ to obtain $\tilde{\mathbf{z}}_{\eta}$, that is, $\tilde{\mathbf{z}}_{\eta} = \tilde{f}_{\eta}(\tilde{\mathbf{z}}_0|k) = \tilde{f}_L \circ \dots \circ \tilde{f}_1(\tilde{\mathbf{z}}_0|k)$, where η are the conditional RealNVP parameters. The distribution of $\tilde{\mathbf{z}}_{\eta}$ is our variational distribution $\tilde{q}_{\eta}(\cdot|k)$, with density

$$\tilde{q}_{\eta}(\tilde{\mathbf{z}}_{\eta}|k) = \tilde{q}_0 \left(\tilde{f}_{\eta}^{-1}(\tilde{\mathbf{z}}_{\eta}|k) \mid k \right) \left| J_{\tilde{f}_{\eta}^{-1}}(\tilde{\mathbf{z}}_{\eta}) \right|. \quad (19)$$

The negative ELBO of our trans-dimensional VI is

$$\begin{aligned} \mathbb{E}_{\tilde{q}_{\eta}(\tilde{\mathbf{z}}_{\eta}, k)} \left[\log \frac{\tilde{q}_{\eta}(\tilde{\mathbf{z}}_{\eta}, k)}{\tilde{\pi}(\tilde{\mathbf{z}}_{\eta}, k, \mathbf{y})} \right] &= \mathbb{E}_{\tilde{q}_{\eta}(\tilde{\mathbf{z}}_{\eta}, k)} \left[\log \frac{\tilde{q}_{\eta}(\tilde{\mathbf{z}}_{\eta}|k)}{\tilde{\pi}(\tilde{\mathbf{z}}_{\eta}, \mathbf{y}|k)} \right] \\ &= \mathbb{E}_{\tilde{q}_0(\tilde{\mathbf{z}}_0, k)} \left[\log \frac{\tilde{q}_{\eta}(\tilde{f}_{\eta}(\tilde{\mathbf{z}}_0|k)|k)}{\tilde{\pi}(\tilde{f}_{\eta}(\tilde{\mathbf{z}}_0|k), \mathbf{y}|k)} \right], \end{aligned} \quad (20)$$

where $\tilde{\pi}(\tilde{\mathbf{z}}_{\eta}, k, \mathbf{y})$ and $\tilde{\pi}(\tilde{\mathbf{z}}_{\eta}, \mathbf{y}|k)$ are the un-normalized versions of $\tilde{\pi}(\tilde{\mathbf{z}}_{\eta}, k|\mathbf{y})$ and $\tilde{\pi}(\tilde{\mathbf{z}}_{\eta}|\mathbf{y}, k)$, the last equation is obtained by applying the reparameterisation trick, and $\tilde{q}_0(\tilde{\mathbf{z}}_0, k) = \tilde{q}_0(\tilde{\mathbf{z}}_0|k)\tilde{q}(k)$. In this paper, we specify $\tilde{q}_0(\cdot|k)$ as $\mathcal{N}_{d_{\max}}(\boldsymbol{\mu}_{\phi}(k), \boldsymbol{\Sigma}_{\phi}(k))$, where both the mean vector $\boldsymbol{\mu}_{\phi}(k)$ and diagonal covariance matrix $\boldsymbol{\Sigma}_{\phi}(k)$ are outputs of MLPs that take k as input. Note that ϕ are the parameters of the MLPs and we train them together with η .

As eq. (20) implies, to optimize the negative ELBO, we only need to draw from the simple distribution $\tilde{q}_0(\tilde{\mathbf{z}}_0, k)$, and avoid sampling from the complex conditional $\pi(\boldsymbol{\theta}_k|\mathbf{y}, k)$ compared to Davies et al. (2023). The training process of the trans-dimensional VI (Algorithm 2 in Appendix A) is similar to Algorithm 1. In each iteration, to estimate the negative ELBO and its gradient, we generate m samples of $(\tilde{\mathbf{z}}_0, k)$ from \tilde{q}_0 . For each sample i , we first draw k^i uniformly from $\{1, 2, \dots, K\}$, and then draw $\tilde{\mathbf{z}}_0^i$ from $\mathcal{N}_{d_{\max}}(\boldsymbol{\mu}_{\phi}(k^i), \boldsymbol{\Sigma}_{\phi}(k^i))$. We specify for each model k a binary mask vector $\boldsymbol{\gamma}_k$ of length d_{\max} , where d_k entries are 1 and others are 0. To compute $\tilde{\pi}(\tilde{\mathbf{z}}_{\eta}, \mathbf{y}|k)$, the entries of $\tilde{\mathbf{z}}_{\eta}$ corresponding to 1 in $\boldsymbol{\gamma}_k$ are used to evaluate the un-normalized conditional posterior $\pi(\cdot, \mathbf{y}|k)$, while the others are to evaluate $\otimes_{d_{\max}-d_k} \nu(\cdot)$.

Using this trans-dimensional VI method with conditional RealNVP, we can obtain the approximate TM for each model k , i.e., $\tilde{T}^{-1}(\cdot|k) = \tilde{f}_{\eta}(\cdot|k)$, by training just once. Generating new proposals of $\boldsymbol{\theta}_k$ works the same as Davies et al. (2023). That is, given $\boldsymbol{\omega} = (k, \boldsymbol{\theta}_k)$, generating $\mathbf{u}_{\sim k}$ from $\otimes_{d_{\max}-d_k} \nu$, sampling k' from $q(\cdot|k)$, and generating $\boldsymbol{\theta}_{k'}$ by $(\boldsymbol{\theta}_{k'}, \mathbf{u}_{\sim k'}) = c_{k'}^{-1} \circ \tilde{T}^{-1}(\cdot|k') \circ \tilde{T}(\cdot|k) \circ c_k(\boldsymbol{\theta}_k, \mathbf{u}_{\sim k})$.

Then $\boldsymbol{\omega}' = (k', \boldsymbol{\theta}_{k'})$ is accepted with probability

$$\alpha(\boldsymbol{\omega}, \boldsymbol{\omega}') = \min \left\{ 1, \frac{\tilde{\pi}(\tilde{\boldsymbol{\theta}}_{k'}, k'|\mathbf{y})q(k|k')|J_{\tilde{T}}(\tilde{\boldsymbol{\theta}}_k|k)|}{\tilde{\pi}(\tilde{\boldsymbol{\theta}}_k, k|\mathbf{y})q(k'|k)|J_{\tilde{T}}(\tilde{\boldsymbol{\theta}}_{k'}|k')|} \right\}, \quad (21)$$

3.3. Within-model Proposals Trained by VI with NFs

If the users are interested in doing within-model updates for a particular model k , we also provide the corresponding TM-based proposals trained by VI with NFs in our framework. Given model k , we train the approximate TM $T_k^{-1} = f_{\eta}$ from $\otimes_{d_k} \nu$ to π_k using the VI method with RealNVP in Section 3.1. Then the within-model update in our framework is similar to the “NeuTraHMC” of Hoffman et al. (2019), proceeding in the following three steps:

1. Transport $\boldsymbol{\theta}_k$ to the reference space via $\mathbf{z}_k = T_k(\boldsymbol{\theta}_k)$;
2. Run MCMC in the reference space, targeting $\pi(\mathbf{z}_k) = \pi(T_k^{-1}(\mathbf{z}_k)|\mathbf{y}, k) |J_{T_k^{-1}}(\mathbf{z}_k)|$;
3. Transform samples of \mathbf{z}_k via T_k^{-1} to obtain samples from $\pi_k = \pi(\cdot|\mathbf{y}, k)$.

Hoffman et al. (2019) used Hamiltonian Monte Carlo (HMC) in Step 2 to sample from $\pi(\mathbf{z}_k)$. If the TM is approximated with high accuracy, $\pi(\mathbf{z}_k)$ would be close to $(\otimes_{d_k} \nu)(\mathbf{z}_k)$, so that simpler MCMC algorithms may also work well. We replace inverse AFs, employed by Hoffman et al. (2019) to approximate TMs, by RealNVP, to reduce the computational cost while preserving expressive power.

3.4. Marginal-Likelihood Estimates from VI with NFs

Given the optimal variational distribution $q_{\eta^*}(\cdot)$ for approximating $\pi(\cdot|\mathbf{y}, k)$ obtained by fitting RealNVP f_{η} , the marginal likelihood for model k , $\pi(\mathbf{y}|k)$, can be estimated using importance sampling, that is,

$$\hat{\pi}(\mathbf{y}|k) = \frac{1}{m} \sum_{i=1}^m \frac{\pi(f_{\eta^*}(\mathbf{z}^i), \mathbf{y}|k)}{q_{\eta^*}(f_{\eta^*}(\mathbf{z}^i))}, \quad (22)$$

for $\mathbf{z}^i \sim \otimes_{d_k} \nu$. Andrade (2024) showed that the VI with RealNVP can yield sharper estimates of marginal likelihoods compared to sequential Monte Carlo (SMC). Accurate marginal likelihood estimates can lead to more efficient model comparison using Bayes factor, which is the ratio of the marginal likelihoods of two compared models. In fact, the estimated ELBO, a direct by-product of our VI method, also serves as an effective model-comparing criterion.

Given that the TMs are exact, if in addition the model-index proposal equals to the posterior model probability,

i.e., $q(k'|k) = \pi(k'|y)$, then the resulting TRJ is rejection-free (Davies et al., 2023). We can use the estimated marginal likelihoods $\{\hat{\pi}(y|k)\}$ to design such a proposal, i.e.,

$$q(k'|k) = \frac{\hat{\pi}(y|k')\pi(k')}{\sum_{k=1}^K \hat{\pi}(y|k)\pi(k)} \quad (23)$$

for $k' \in \{1, 2, \dots, K\}$, which is supposed to be close to $\pi(k'|y)$, since $\pi(k|y) = \frac{\pi(y|k)\pi(k)}{\pi(y)}$.

4. Numerical Experiments

In this section, we use the numerical examples of Davies et al. (2023) to compare the performance of our new method to existing baselines. We also use the same two MCMC diagnoses as Davies et al. (2023), that is, the running estimates of posterior model probabilities, and the *Bartolucci Bridge Estimator* (BBE) for model probabilities. The BBE (Bartolucci et al., 2006) approximates the Bayes factor between models k and k' using the ratio of the estimated average acceptance probabilities for the two models, i.e., $\hat{B}_{k,k'} = (N_{k'}^{-1} \sum_{i=1}^{N_{k'}} \alpha'_i) / (N_k^{-1} \sum_{i=1}^{N_k} \alpha_i)$, where $N_{k'}$ and N_k are the total numbers of proposals from model k' to k , and from k to k' respectively in the algorithm, and α'_i and α_i are the acceptance probabilities calculated for each $k' \rightarrow k$ and $k \rightarrow k'$ proposals. Under uniform model-index prior, it is simple to convert $\hat{B}_{k,k'}$ s to estimates of model probabilities (Bartolucci et al., 2006), i.e., $\hat{\pi}(k|y) = \hat{B}_{jk}^{-1} (1 + \sum_{i=1, i \neq j}^K \hat{B}_{i,j})^{-1}$ for arbitrary $j \in \{1, 2, \dots, K\}$. As Davies et al. (2023), we use an evaluation set of N samples per model which is independent of the burn-in period, and generate one reversible jump proposal per sample to obtain the $\hat{B}_{k,k'}$ s for computing $\hat{\pi}(k|y)$.

4.1. Illustrative Example

As Davies et al. (2023), we first consider a toy example where the trans-dimensional target consists of two models with dimensions $d_1 = 1$ and $d_2 = 2$ respectively, each of which is constructed via the pushforward of a Gaussian distribution through the (element-wise) inverse sinh-arcsinh (SAS) transformation (Jones & Pewsey, 2009), that is, $S_{\epsilon, \delta}(\cdot) = \sinh(\delta^{-1} \odot (\sinh^{-1}(\cdot) + \epsilon))$, where $\epsilon \in \mathbb{R}^d$ and $\delta \in \mathbb{R}_+^d$. For $z \sim \mathcal{N}_d(\mathbf{0}, \mathbf{I}_d)$ and an $d \times d$ matrix \mathbf{L} , the transformation is defined by $T(z) = S_{\epsilon, \delta}(\mathbf{L}z)$, and the induced density of $\theta = T(z)$ is $\pi_{\epsilon, \delta, \mathbf{L}}(\theta) = \phi_{\mathbf{L}\mathbf{L}^\top}(S_{\epsilon, \delta}^{-1}(\theta)) |J_{S_{\epsilon, \delta}^{-1}}(\theta)|$, where $\phi_{\mathbf{L}\mathbf{L}^\top}(\cdot)$ is the density of the Gaussian distribution $\mathcal{N}_d(\mathbf{0}, \mathbf{L}\mathbf{L}^\top)$ and $S_{\epsilon, \delta}^{-1}(\cdot) = \sinh(\delta \odot \sinh^{-1}(\cdot) - \epsilon)$. The prior for models are $\frac{1}{4}$ for $k = 1$ and $\frac{3}{4}$ for $k = 2$, so that the joint target is

$$\pi(k, \theta_k) = \begin{cases} \frac{1}{4} \pi_{\epsilon_1, \delta_1, \mathbf{L}_1}(\theta_1), & k = 1, \\ \frac{3}{4} \pi_{\epsilon_2, \delta_2, \mathbf{L}_2}(\theta_2), & k = 2, \end{cases} \quad (24)$$

where $\epsilon_1 = -2$, $\delta_1 = 1$, $\mathbf{L}_1 = 1$, $\epsilon_2 = (1.5, -2)$, $\delta_2 = (1, 1.5)$, and \mathbf{L}_2 is such a lower-triangular matrix that

$$\mathbf{L}_2 \mathbf{L}_2^\top = \begin{bmatrix} 1 & 0.99 \\ 0.99 & 1 \end{bmatrix}. \quad (25)$$

We approximate the TMs for the two models in the TRJ proposals using the four NFs below: (1) affine flows, (2) RQMA, (3) planar flows for model $k = 1$ and RealNVP for $k = 2$, and (4) exact map. The flow depths in (3) are chosen using ablation study (fig. 6 in Appendix B.1). In this example, we train the approximate TM for each model individually. We fit each of (1) and (2) using $N = 5 \times 10^4$ exact samples per model as Davies et al. (2023). For (3), we fit the TMs using the VI method with NFs introduced in Section 3.1. Figure 1 shows the TRJ proposals learned using all the methods above. Compared to the TRJ with exact map, our VI with RealNVP provides more accurate TM approximation than the affine and RQMA flows fit with samples from the target.

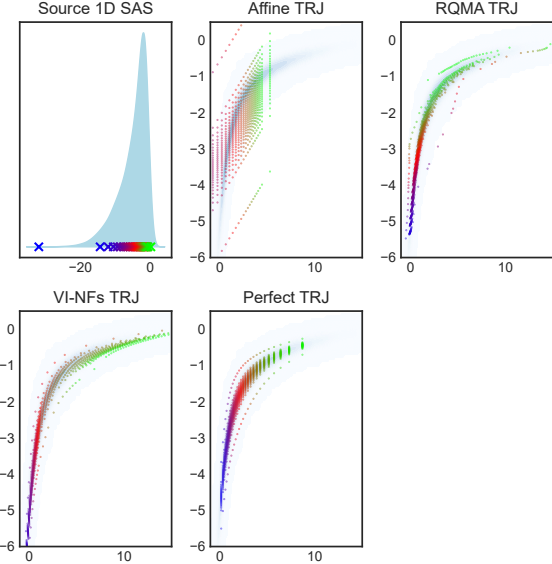


Figure 1. Systematic draws from the conditional $\pi(\theta_1|k = 1)$ of the target in eq. (24) (top left) are transported to the state space of $\pi(\theta_2|k = 2)$ using each of the TRJ proposals with affine map (top middle), RQMA map (top right), RealNVP map (bottom left), and exact map (bottom middle). Affine and RQMA are fit as in Davies et al. (2023) while RealNVP fit using VI. Auxiliary variables are also sampled systematically.

To sample from $\pi(k, \theta_k)$ in eq. (24), we consider RJMCMC with the TRJ proposals learned using each of the four methods above. For each RJMCMC, we follow Davies et al. (2023) and set the model-index proposal to be $q(k'|k) = \frac{1}{4} \mathbb{I}_{\{k'=1\}} + \frac{3}{4} \mathbb{I}_{\{k'=2\}}$ for $k \in \{1, 2\}$, where $\mathbb{I}_{\{\cdot\}}$ equals to 1 if the condition in brackets is satisfied and 0 otherwise. Figure 2 visualizes the running estimates of probability for model $k = 2$ from each of the four algorithms

against ground truth $\frac{3}{4}$. Our algorithm exhibits comparable performance to RJMCMC with exact map, converging much faster than the two algorithms of Davies et al. (2023).

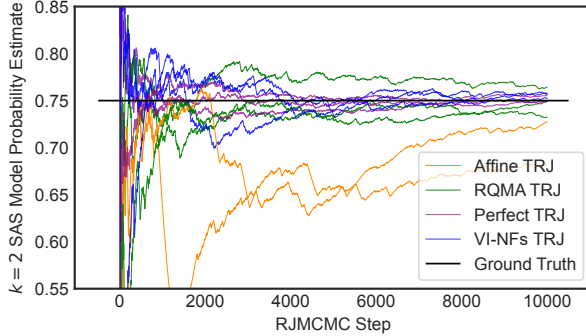


Figure 2. Running estimates of the probability for model $k = 2$ in the target of eq. 24 from RJMCMC using TRJ proposals with affine map (yellow), RQMA (green), RealNVP fit by VI (blue) and exact map (purple). Three chains are run for each RJMCMC.

4.2. Bayesian Factor Analysis

The data are monthly exchange rates of six currencies relative to British pound, spanning from January 1975 to December 1986 (Lopes & West, 2004) as 143 observations, denoted by $\mathbf{y}_i \in \mathcal{R}^6$ for $i = 1, 2, \dots, 143$. We consider the factor analysis model where $\mathbf{y}_i \sim \mathcal{N}_6(\mathbf{0}, \boldsymbol{\Sigma})$ and $\boldsymbol{\Sigma} = \boldsymbol{\beta}_k \boldsymbol{\beta}_k^\top + \boldsymbol{\Lambda}$, with $\boldsymbol{\Lambda}$ to be a 6×6 positive diagonal matrix, $\boldsymbol{\beta}_k = [\beta_{ij}]$ a $6 \times k$ lower-triangular matrix with strictly positive diagonal entries, and k the number of factors. The parameter vector $\boldsymbol{\theta}_k = (\boldsymbol{\beta}_k, \boldsymbol{\Lambda})$ of the model has a dimension of $6(k+1) - k(k-1)/2$. As Davies et al. (2023), we assign the following priors to $\boldsymbol{\theta}_k$: $\beta_{ij} \sim \mathcal{N}(0, 1)$ for $i > j$, $\beta_{jj} \sim \mathcal{N}_+(0, 1)$, and $\boldsymbol{\Lambda}_{ii} \sim \mathcal{IG}(1.1, 0.05)$ where $i = 1, \dots, 6$, $j = 1, \dots, k$ and \mathcal{IG} is the inverse Gamma distribution, and also consider the posterior of $\boldsymbol{\theta}_k$ with $k = 2$ or 3 factors so that the joint posterior is

$$\pi(k, \boldsymbol{\theta}_k | \mathbf{y}) \propto \prod_{i=1}^{143} \phi_{\boldsymbol{\beta}_k \boldsymbol{\beta}_k^\top + \boldsymbol{\Lambda}}(\mathbf{y}_i) \pi(\boldsymbol{\beta}_k | k) \pi(\boldsymbol{\Lambda}) \pi(k), \quad (26)$$

where $\mathbf{y} = (\mathbf{y}_1, \mathbf{y}_2, \dots, \mathbf{y}_{143})$, $\pi(\boldsymbol{\beta}_k | k)$ and $\pi(\boldsymbol{\Lambda})$ are the priors above and $\pi(k) = \frac{1}{2}$ for $k = 2$ or 3.

To sample from the target in eq. (26), we consider RJMCMC with each of the four proposals, that is, (1) independent proposal $q(\boldsymbol{\theta}_k) = q(\boldsymbol{\beta}_k) \prod_{j=1}^6 q(\boldsymbol{\Lambda}_{jj})$ with parameters estimated using samples from the conditional targets (Lopes & West, 2004), (2) TRJ proposal with affine map trained using samples from the target, (3) TRJ proposal with RQMA map trained using target samples, and (4) TRJ proposal with RealNVP map fit by VI as in Section 3.1. For (4), the flow depth is chosen with ablation study (fig. 7 in Appendix B.1) and parameter positivity is enforced via softplus

transforms (Kucukelbir et al., 2017). As Davies et al. (2023), to obtain training samples for proposals (1)–(3) and evaluation sets to compute BBEs for all the methods, we use No-U-Turn Sampler (NUTS) (Hoffman & Gelman, 2014) in PyMC (Salvatier et al., 2016) for the 3-factor model, and static temperature-annealed SMC (Moral et al., 2006) for the 2-factor model. The size of the evaluation set is identical to the training set, with both $N = 2 \times 10^3$ and $N = 1.6 \times 10^4$ per model considered. For each N , 10 pairs of training and evaluation sets are generated, and evaluations are conducted 100 times per set, yielding a total of 1000 BBEs.

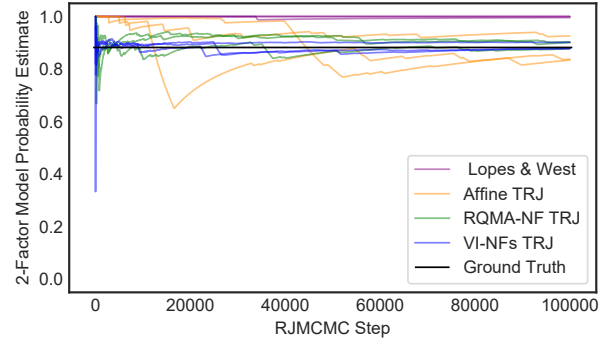


Figure 3. Running estimates of the model probability for the 2-factor model in the target of eq. (26), obtained by RJMCMC with the independent proposal (purple), TRJ proposal with affine map (yellow), TRJ with RQMA map (green), and TRJ with RealNVP map fit by VI (blue). Three chains are run for each algorithm.

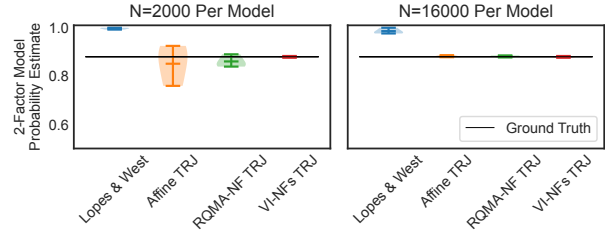


Figure 4. Violin plot for factor analysis, showing the variability of the 2-factor model probability estimates obtained using BBEs.

Figure 3 compares the running estimates of posterior model probability for the 2-factor model from RJMCMC using the proposals (1)–(4) against the ground truth 0.88 reported by (Lopes & West, 2004). Each RJMCMC is run for 10^5 iterations. Our method again shows faster convergence. Figure 4 shows the variability of model probability estimates obtained by BBE. Our method produces more accurate estimates with less variance compared to (1)–(3). In fact the TRJ proposal with RealNVP map fit by VI approximates the target with much better accuracy (fig. 8 in Appendix B.2).

4.3. Variable Selection in Robust Regression Analysis

The regression model [Davies et al. \(2023\)](#) considered is $\mathbf{Y} = \mathbf{X}\beta + \epsilon$, where $\mathbf{Y} = (Y_1, Y_2, \dots, Y_{80})$, each Y_i has a vector of covariates $(x_{i0}, x_{i1}, x_{i2}, x_{i3})$ with $x_{i0} = 1$, \mathbf{X} is the corresponding design matrix, $\beta = (\beta_0, \beta_1, \beta_2, \beta_3)$ and $\epsilon = (\epsilon_1, \epsilon_2, \dots, \epsilon_{80})$ are the error terms, independently and identically distributed to a mixture of $\mathcal{N}(0, 1)$ and $\mathcal{N}(0, 100)$, thereby providing robustness to outliers. Following [Davies et al. \(2023\)](#), we extend the model index k to an binary vector of dimension 4, where the i th position is 1 if β_i is included in the model and 0 otherwise. We adopt the same priors as [Davies et al. \(2023\)](#), that is, $k_j \sim \text{Bernoulli}(\frac{1}{2})$ for $j = 1, 2$, and $\beta_l \sim \mathcal{N}(0, 100)$ for $l = 0, 1, 2, 3$. The target distribution π is the joint posterior of the model indicator k and the corresponding regression coefficients θ_k , which is a sub-vector of β . As [Davies et al. \(2023\)](#), we consider models of the form $k = (1, k_1, k_2, k_3)$, that is, β_1 is always included, β_2 and β_3 are included or excluded jointly, so that there are 4 candidate models in total.

The data for this example are simulated using $k = (1, 1, 0, 0)$, so that $\theta_k = (\beta_0, \beta_1)$. As [Davies et al. \(2023\)](#), we simulate half of the \mathbf{Y} observations using $(\beta_0, \beta_1) = (1, 1)$ and the other half using $(\beta_0, \beta_1) = (6, 1)$, to introduce challenging multimodal features into the posterior. The entries of \mathbf{X} are drawn from $\mathcal{N}(0, 1)$, and ϵ_i s from $\mathcal{N}(0, 25)$.

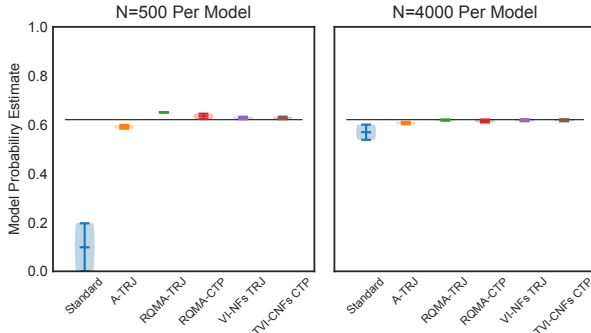


Figure 5. Violin plots showing the variability of the $k = (1, 1, 1, 1)$ model probability estimated using BBE for each RJMCMC against a ground truth from 5×10^4 SMC particles. Here “A-TRJ”, “ROMA-TRJ” and “ROMA-CTP” correspond to RJMCMC with affine-map TRJ, ROMA-map TRJ and ROMA-map CTP, all fit using samples from the target. “VI-NFs TRJ” and “TVI-CNFs CTP” correspond to RJMCMC with RealNVP-map TRJ and CTP fit using (trans-dimensional) VI.

To sample from the posterior, we consider six RJMCMC algorithms, that is, (1) the independence auxiliary sampler of [Brooks et al. \(2003\)](#), named “standard” by [Davies et al. \(2023\)](#), which uses the augmented target as eq. (7) with ν to be $\mathcal{N}(0, 100)$, so that the proposal is deterministic and works by switching i th parameter block on or off, depending

on whether $k_i = 1$ or 0; (2) RJMCMC with affine-map TRJ proposal fit using samples from the target; (3) RJMCMC with ROMA-map TRJ fit using target samples; (4) RJMCMC with ROMA-map CTP fit “all-in-one” using target samples; (5) RJMCMC with RealNVP-map TRJ fit using VI; (6) RJMCMC with RealNVP-map CTP fit “all-in-one” using trans-dimensional VI with conditional NFs in Section 3.2. Note that here we consider both TRJ proposals with TMs fit individually and CTP where all the TMs are fit by training once. Algorithms (1)–(4) were considered in [Davies et al. \(2023\)](#). The performance is assessed using BBE, with the evaluation set to be the same size as the training set for proposals in (2)–(4), and we consider $N = 500, 1000, 2000, 4000$ samples per model drawn from a single SMC run. For each N , 80 BBEs are generated.

Figure 5 shows the variability of the $k = (1, 1, 1, 1)$ model probability estimated using BBE with $N = 500$ and 4000 . See figure 9 of Appendix B.2 for the results of other models and N values. RJMCMC with TRJ proposals are much more efficient than the standard sampler and our VI with RealNVP further improves the estimation accuracy of TRJ proposals. Particularly the CTP fit using our trans-dimensional VI with conditional RealNVP performs better than the CTP trained using target samples as [Davies et al. \(2023\)](#).

5. Discussion

Our framework using VI with (conditional) NFs to train both between-model and within-model TM-based proposals for RJMCMC does not require pilot samples from the complex target. Using RealNVP rather than AFs to approximate TMs makes the computation highly parallelisable while maintaining comparable expressive power. Numerical studies show that our method leads to more accurate approximation of TMs and faster convergence of the corresponding RJMCMC. Especially the CTP trained by our trans-dimensional VI with conditional NFs produces more accurate estimates of model probabilities with less variance compared to the CTP trained using target samples. A future avenue of research is to design high-acceptance or rejection-free trans-dimensional proposals, which can be naturally achieved under our framework, since accurate marginal-likelihood estimates are by-products and using them can produce proposals for model index k close to the posterior probabilities. Furthermore, it is possible to expand our trans-dimensional VI with conditional NFs to a VI method targeting $\pi(k, \theta_k | \mathbf{y})$ by adding inference for k .

References

Al-Awadhi, F., Hurn, M., and Jennison, C. Improving the acceptance rate of reversible jump MCMC proposals. *Statistics & Probability Letters*, 69(2):189–198, 2004.

Andrade, D. Stabilizing training of affine coupling layers for high-dimensional variational inference. *Machine Learning: Science and Technology*, 5(4):045066, 2024.

Bartolucci, F., Scaccia, L., and Mira, A. Efficient bayes factor estimation from the reversible jump output. *Biometrika*, 93(1):41–52, 2006.

Blei, D. M., Kucukelbir, A., and McAuliffe, J. D. Variational inference: A review for statisticians. *Journal of the American Statistical Association*, 112(518):859–877, 2017.

Brooks, S. P., Giudici, P., and Roberts, G. O. Efficient construction of reversible jump Markov chain Monte Carlo proposal distributions. *Journal of the Royal Statistical Society: Series B*, 65(1):3–39, 2003.

Davies, L., Salomone, R., Sutton, M., and Drovandi, C. Transport reversible jump proposals. In *Proceedings of the 26th International Conference on Artificial Intelligence and Statistics*, pp. 6839–6852, 2023.

Dinh, L., Sohl-Dickstein, J., and Bengio, S. Density estimation using real NVP. In *International Conference on Learning Representations*, 2017.

Durkan, C., Bekasov, A., Murray, I., and Papamakarios, G. nflows: Normalizing flows in PyTorch. Zenodo, 2020.

Fan, Y., Peters, G. W., and Sisson, S. A. Automating and evaluating reversible jump MCMC proposal distributions. *Statistics and Computing*, 19(4):409–421, 2009.

Fan, Y., Sisson, S. A., and Davies, L. Reversible jump Markov chain Monte Carlo and multi-model samplers. In *Handbook of Markov Chain Monte Carlo*. Chapman and Hall/CRC, 2026.

Farr, W. M., Mandel, I., and Stevens, D. An efficient interpolation technique for jump proposals in reversible-jump Markov chain Monte Carlo calculations. *Royal Society Open Science*, 2(6):150030, 2015.

Gabrié, M., Rotskoff, G. M., and Vanden-Eijnden, E. Efficient Bayesian sampling using normalizing flows to assist Markov chain Monte Carlo methods. In *ICML Workshop on Invertible Neural Networks, Normalizing Flows, and Explicit Likelihood Models*, 2021.

Gagnon, P. Informed reversible jump algorithms. *Electronic Journal of Statistics*, 15(2), 2021.

GREEN, P. J. Reversible jump Markov chain Monte Carlo computation and bayesian model determination. *Biometrika*, 82(4):711–732, 1995.

Green, P. J. Trans-dimensional Markov chain Monte Carlo. In *Highly Structured Stochastic Systems*, pp. 179–198. Oxford University Press, 2003.

Green, P. J. and Mira, A. Delayed rejection in reversible jump Metropolis–Hastings. *Biometrika*, 88(4):1035–1053, 2001.

Hoffman, M., Sountsov, P., Dillon, J. V., Langmore, I., Tran, D., and Vasudevan, S. NeuTra-lizing bad geometry in Hamiltonian monte Carlo using neural transport. arXiv preprint, 2019.

Hoffman, M. D. and Gelman, A. The no-U-turn sampler: Adaptively setting path lengths in Hamiltonian monte Carlo. *Journal of Machine Learning Research*, 15(47):1593–1623, 2014.

Jiao, X., Flouri, T., and Yang, Z. Multispecies coalescent and its applications to infer species phylogenies and cross-species gene flow. *National Science Review*, 8(12):nwab127, 2021.

Jones, M. C. and Pewsey, A. Sinh-arcsinh distributions. *Biometrika*, 96(4):761–780, 2009.

Kingma, D. P. and Ba, J. Adam: A method for stochastic optimization. In *International Conference on Learning Representations*, 2015.

Kingma, D. P. and Welling, M. Auto-encoding variational bayes. In *The 2nd International Conference on Learning Representations*, 2014.

Koehler, F., Mehta, V., and Risteski, A. Representational aspects of depth and conditioning in normalizing flows. In *Proceedings of the 38th International Conference on Machine Learning*, pp. 5628–5636, 2021.

Kucukelbir, A., Tran, D., Ranganath, R., Gelman, A., and Blei, D. M. Automatic differentiation variational inference. *Journal of Machine Learning Research*, 18(14):1–45, 2017.

Lopes, H. F. and West, M. Bayesian model assessment in factor analysis. *Statistica Sinica*, 14(1):41–67, 2004.

Moral, P. D., Doucet, A., and Jasra, A. Sequential Monte Carlo samplers. *Journal of the Royal Statistical Society: Series B*, 68(3):411–436, 2006.

Papamakarios, G., Pavlakou, T., and Murray, I. Masked autoregressive flow for density estimation. In *Advances in Neural Information Processing Systems*, pp. 2338–2347, 2017.

Parno, M. D. and Marzouk, Y. M. Transport map accelerated Markov chain Monte Carlo. *SIAM/ASA Journal on Uncertainty Quantification*, 6(2):645–682, 2018.

Rezende, D. and Mohamed, S. Variational inference with normalizing flows. In *Proceedings of the 32nd International Conference on Machine Learning*, pp. 1530–1538, 2015.

Salvatier, J., Wiecki, T. V., and Fonnesbeck, C. Probabilistic programming in python using PyMC3. *PeerJ Computer Science*, 2:e55, 2016.

Sambridge, M., Bodin, T., Gallagher, K., and Tkalcic, H. Transdimensional inference in the geosciences. *Philosophical Transactions of the Royal Society A: Mathematical, Physical and Engineering Sciences*, 371(1984):20110547, 2013.

A. Algorithms and Experimental Details

We show in Algorithm 2 the procedure of using trans-dimensional VI to train the TMs specified with conditional RealNVP, which was introduced in Section 3.2 of the main text, and present one iteration of our complete RJMCMC algorithm in Algorithm 3.

Algorithm 2 Stochastic Gradient Descent for Trans-dimenisonal VI with Conditional RealNVP

```

1: Set the iteration  $t \leftarrow 1$  and negative ELBO  $\ell^{(t)} \leftarrow \infty$ 
2: Initialize  $\boldsymbol{\eta}^{(t)}$ 
3: Initialize optimizer  $\mathcal{P}$  with global learning rate  $\boldsymbol{\xi}^{(0)}$ 
4: repeat
5:   Sample  $k^i$  uniformly from  $\{1, 2, \dots, K\}$  and  $\tilde{\mathbf{z}}^i \sim \mathcal{N}_{d_{\max}}(\boldsymbol{\mu}_{\phi}(k^i), \boldsymbol{\Sigma}_{\phi}(k^i))$ , for  $i = 1, \dots, m$ ;
6:    $\mathbf{g}^{(t)} \leftarrow \frac{1}{m} \sum_{i=1}^m \left[ \frac{\partial}{\partial \boldsymbol{\eta}} \log \frac{\tilde{q}_{\boldsymbol{\eta}^{(t)}}(\tilde{\mathbf{z}}^i | k^i) | k^i}{\tilde{\pi}(\tilde{\mathbf{f}}_{\boldsymbol{\eta}^{(t)}}(\tilde{\mathbf{z}}^i | k^i), \mathbf{y} | k^i)} \right]$ 
7:   Update the learning rate  $\boldsymbol{\xi}^{(t)}$  and direction  $\Delta \boldsymbol{\eta}^{(t)}$  with  $\mathcal{P}$  using  $\mathbf{g}^{(t)}$ 
8:    $\boldsymbol{\eta}^{(t+1)} \leftarrow \boldsymbol{\eta}^{(t)} + \boldsymbol{\xi}^{(t)} \Delta \boldsymbol{\eta}^{(t)}$ 
9:    $\ell^{(t+1)} \leftarrow \frac{1}{m} \sum_{i=1}^m \left[ \log \frac{\tilde{q}_{\boldsymbol{\eta}^{(t+1)}}(\tilde{\mathbf{z}}^i | k^i) | k^i}{\tilde{\pi}(\tilde{\mathbf{f}}_{\boldsymbol{\eta}^{(t+1)}}(\tilde{\mathbf{z}}^i | k^i), \mathbf{y} | k^i)} \right]$ 
10:   $t \leftarrow t + 1$ 
11: until  $t > \text{max-iterations}$ 

```

Algorithm 3 RJMCMC with TM-based Proposals Trained Using VI with (Conditional) NFs (one iteration)

Input: Current state $\boldsymbol{\omega} = (k, \boldsymbol{\theta}_k)$, and

1: Target $\pi(\boldsymbol{\omega} | \mathbf{y})$;
2: Model-index proposal $q(\cdot | k)$;
3: Reference distribution ν ;
4: Transport maps $\{T_k\}_{k=1}^K$ from π_k to $\otimes_{d_k} \nu$ either specified using RealNVP and fit using standard VI as Algorithm 1, or specified using conditional RealNVP and fit using trans-dimensional VI as Algorithm 2;
5: User-specified within-model update index $\mathbb{I}_{\text{within}}$ (0 or 1); if $\mathbb{I}_{\text{within}} = 1$, specify an within-model MCMC algorithm \mathcal{A} ;

Output: New state $\boldsymbol{\omega}' = (k', \boldsymbol{\theta}'_k)$

```

6:  $k' \sim q(\cdot | k)$ 
7:  $\mathbf{z}_k \leftarrow T_k(\boldsymbol{\theta}_k)$ 
8: if  $d_{k'} \geq d_k$  then
9:   Draw  $\mathbf{u}_k \sim \otimes_{d_{k'} - d_k} \nu$ ;  $g_u \leftarrow (\otimes_{d_{k'} - d_k} \nu)(\mathbf{u}_k)$ ;  $g'_u \leftarrow 1$ ;  $\mathbf{z}_{k'} \leftarrow \bar{h}_{k, k'}(\mathbf{z}_k, \mathbf{u}_k)$ 
10: else
11:    $(\mathbf{z}_{k'}, \mathbf{u}_{k'}) \leftarrow \bar{h}_{k, k'}^{-1}(\mathbf{z}_k)$ ; discard  $\mathbf{u}_{k'}$ ;  $g_u \leftarrow 1$ ;  $g'_u \leftarrow (\otimes_{d_k - d_{k'}} \nu)(\mathbf{u}_{k'})$ 
12: end if
13:  $\boldsymbol{\theta}'_{k'} \leftarrow T_{k'}^{-1}(\mathbf{z}_{k'})$ 
14:  $\boldsymbol{\omega}' \leftarrow (k', \boldsymbol{\theta}'_{k'})$ ;  $\alpha \leftarrow 1 \wedge \frac{\pi(\boldsymbol{\omega}') q(k | k') g'_u}{\pi(\boldsymbol{\omega}) q(k' | k) g_u} |J_{T_k}(\boldsymbol{\theta}_k)| |J_{T_{k'}}(\boldsymbol{\theta}'_{k'})|^{-1}$ 
15: Draw  $V \sim \mathcal{U}(0, 1)$ 
16: if  $\alpha > V$  then
17:    $\boldsymbol{\omega}' \leftarrow \boldsymbol{\omega}'$ 
18: else
19:    $\boldsymbol{\omega}' \leftarrow \boldsymbol{\omega}$ 
20: end if
21: if  $\mathbb{I}_{\text{within}} = 1$  then
22:    $\mathbf{z}'_k \leftarrow T_k(\boldsymbol{\theta}'_k)$ ; update  $\mathbf{z}'_k$  via  $\mathcal{A}$  for target  $\pi(T_k^{-1}(\mathbf{z}'_k) | \mathbf{y}, k) |J_{T_k^{-1}}(\mathbf{z}'_k)|$ ;  $\boldsymbol{\theta}'_k \leftarrow T_k^{-1}(\mathbf{z}'_k)$ 
23: end if

```

In our numerical examples, we specified scale function s and translation function t in each RealNVP transformation as a MLP with one hidden layer of size 256. The Leaky ReLU was used as the activation function. All network parameters were initialized with 0. We train all VI with NFs used in our numerical examples by employing Adam optimizer (Kingma & Ba,

2015) with a mini-batch of size 256 and a fixed learning rate of 10^{-4} . We set the maximum number of training iterations to be 10,000 across all experiments, except for the algorithm fitting the trans-dimensional VI with conditional RealNVP in the example of Section 4.3, for which we set the maximum to 40,000 iterations, since four flow models with different dimensions are trained simultaneously in this algorithm. Mostly, training converged before reaching the maximum number of iterations. Therefore we implemented early stopping criteria in the SGVI algorithms to improve computational efficiency. We used the same hyper-parameter settings for other baseline algorithms as Davies et al. (2023) to ensure a fair comparison. Implementation details and source code are available at: <https://github.com/Palantir-zoe/vinftrjp>.

B. Ablation Study and Supplementary Numerical Results

B.1. Ablation Study

We used the ablation studies to investigate the effect of the RealNVP depth on the performance of our RJMCMC algorithm which uses VI with NFs to train the TRJ proposals. The results are shown in figure 6 for the illustrative example in Section 4.1 and figure 7 for the factor-analysis example in Section 4.2, with the running estimates of model probabilities visualised for the algorithms with TMs specified by RealNVP with different depths. For the illustrative example, the optimal depth we used in the experiments for the main text are $L = 8$ for model $k = 1$ and $L = 9$ for model $k = 2$, and we used $L = 16$ for both the 2-factor and 3-factor models in the factor-analysis example.

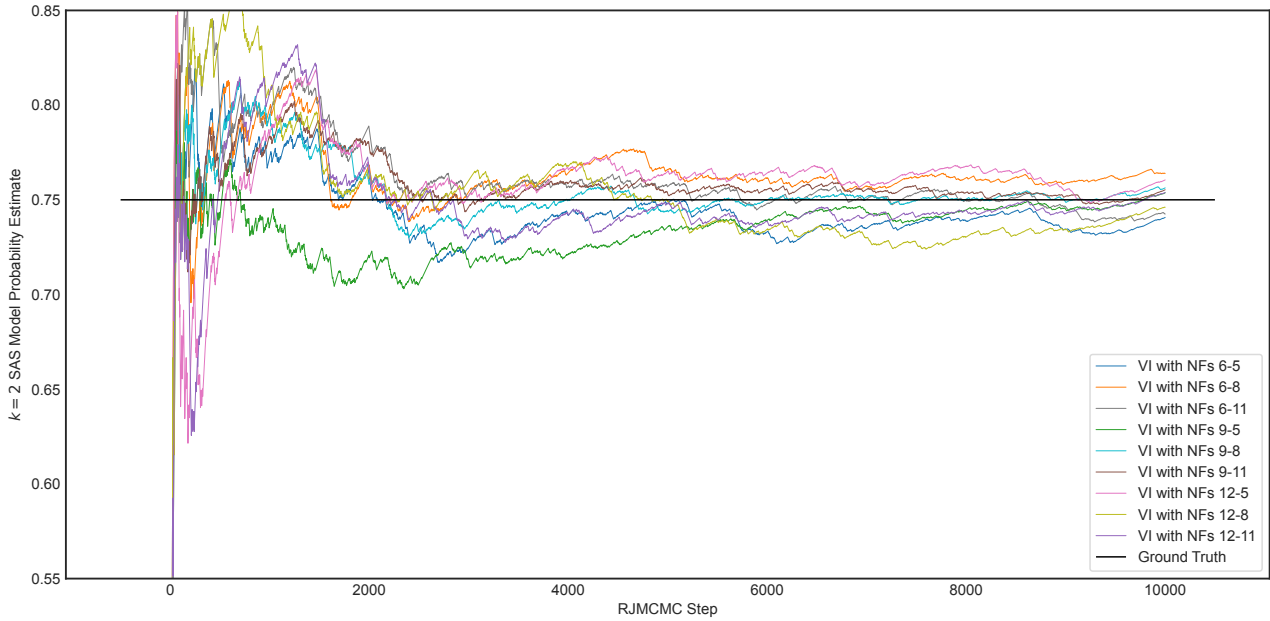


Figure 6. The results of the ablation study for the illustrative example in Section 4.1

B.2. Supplementary Numerical Results

In this section, we show some supplementary results for the factor-analysis examples in Section 4.2 and the variable-selection example in Section 4.3. For factor analysis, we show in figure 8 a visualization (using selected bivariate plots) of the proposal from points on the 2-factor model to proposed points on the 3-factor model for each of the four proposal types mentioned in the main text of Section 4.2, against a ground-truth kernel density estimated using 5×10^4 SMC particles. The TRJ proposal with RealNVP map fit by VI approximates the target with the best accuracy. For variable selection, we visualize in figure 9 the variability of model probabilities estimated using BBE for each of the six RJMCMC algorithms mentioned in the main text of Section 4.3 across both the 4 candidate models and the four N values. The results are consistent across models and N values, that is, RJMCMC with TRJ proposals are much more efficient than the standard sampler, our VI with RealNVP further improves the estimation accuracy of TRJ proposals, and the CTP fit using our trans-dimensional VI with conditional RealNVP performs better than the CTP trained using target samples as Davies et al. (2023).

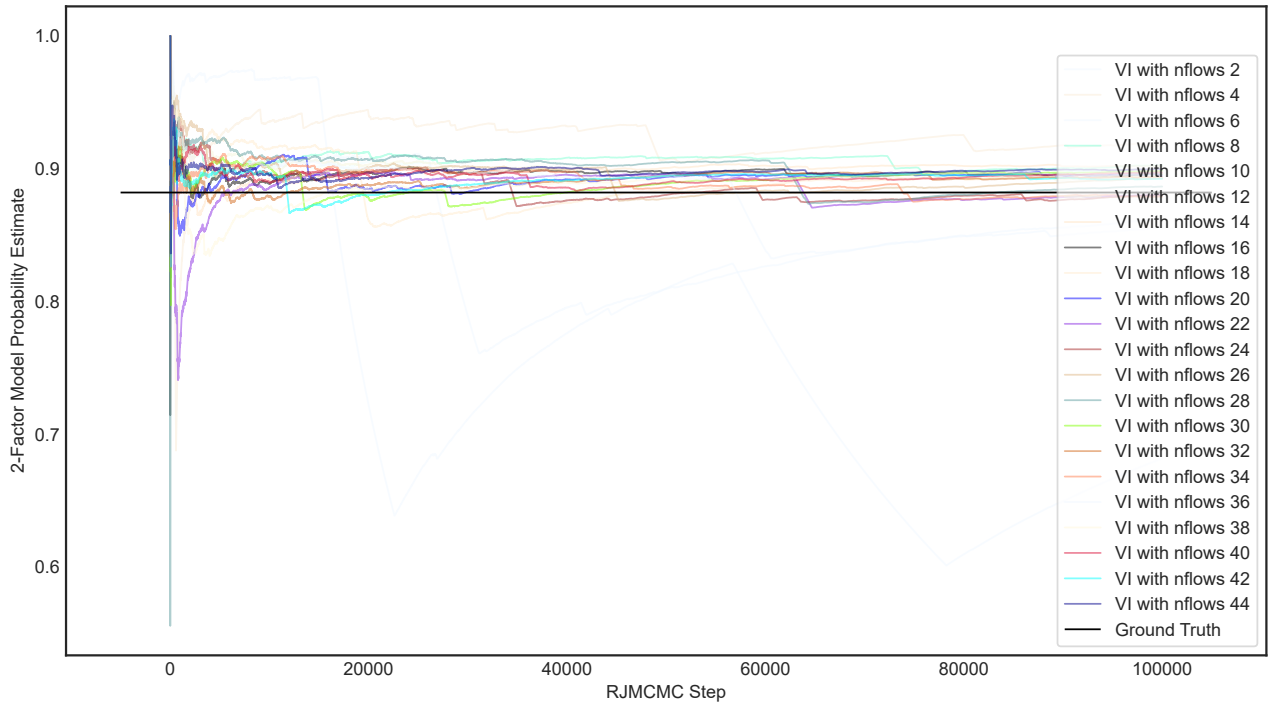


Figure 7. The results of the ablation study for the factor-analysis example in Section 4.2.

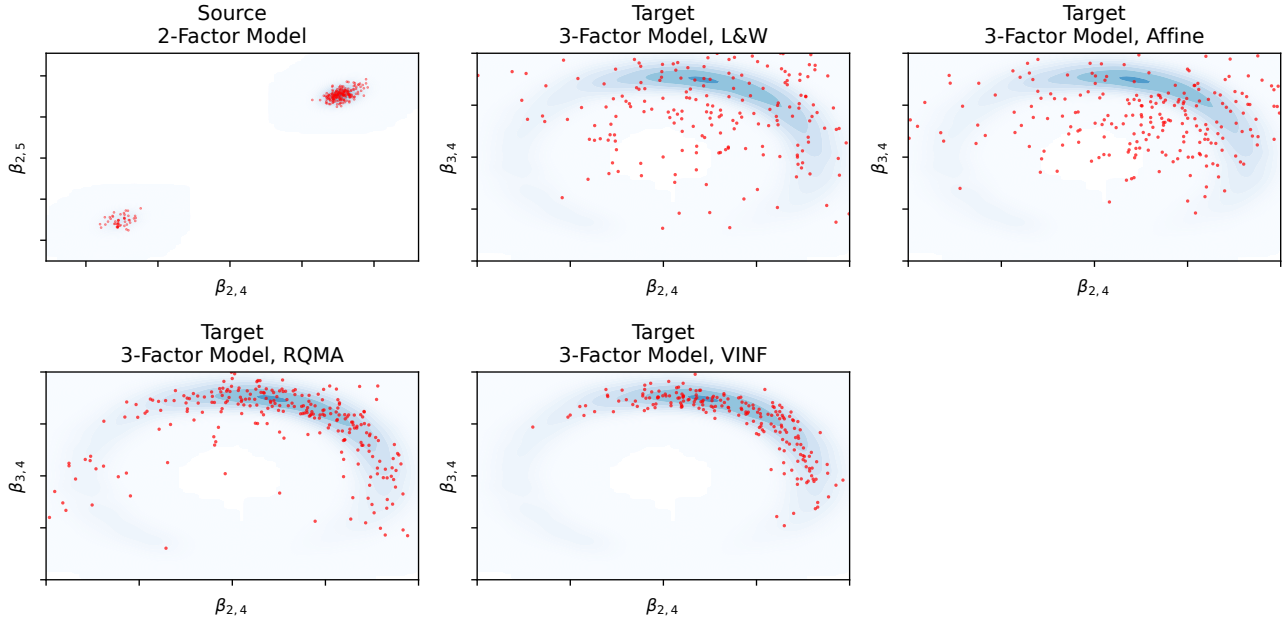


Figure 8. A visualization (using selected bivariate plots) of the proposal from points on the 2-factor model (top-left) to proposed points on the 3-factor model for each proposal type: independent proposal (top middle); TRJ with affine map (top right); TRJ with RQMA (bottom left) and TRJ with RealNVP fit by VI (bottom middle). Ground truth kernel densities (light blue) are estimated using 5×10^4 individual SMC particles.

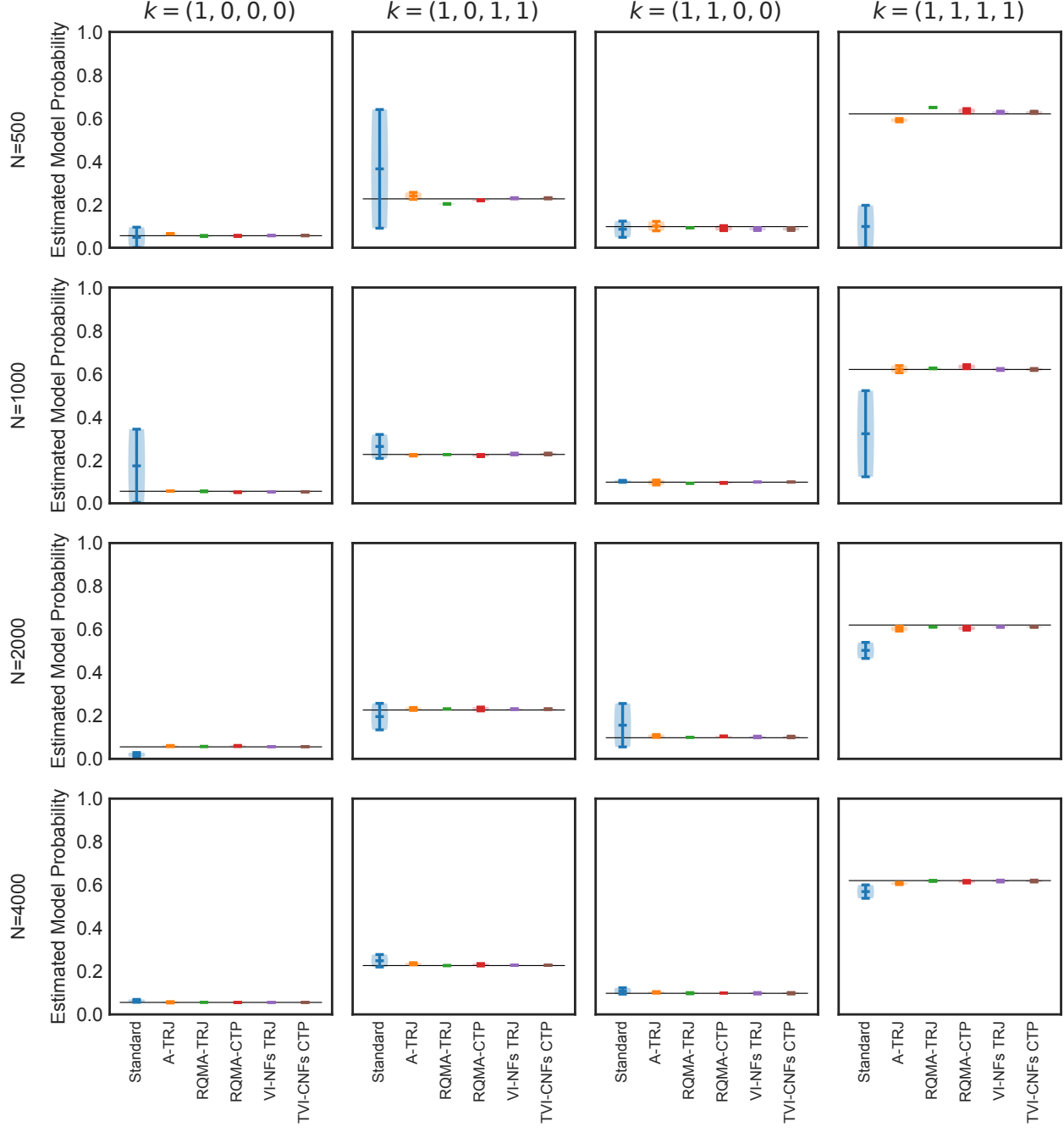


Figure 9. Violin plots showing the variability for each of the 4 model probabilities estimated using BBE with $N = 500, 1000, 2000$, and 4000 respectively for each RJMCMC against a ground truth from 5×10^4 SMC particles. Here “A-TRJ”, “RQMA-TRJ” and “RQMA-CTP” correspond to RJMCMC with affine-map TRJ, RQMA-map TRJ and RQMA-map CTP, all fit using samples from the target. “VI-NFs TRJ” and “TVI-CNFs CTP” correspond to RJMCMC with RealNVP-map TRJ and CTP fit using (trans-dimensional) VI.